Intermetallics 142 (2022) 107467

Contents lists available at ScienceDirect

Intermetallics

journal homepage: www.elsevier.com/locate/intermet

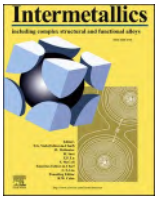

Fast increase in ductility and strength of Zr-based bulk amorphous alloys induced by intermittent high-frequency vibration loading

Yan Lou [a,*], Lingyun Yang [a], Shenpeng Xv [a,b], Jiang Ma [a]

[a] Shenzhen Key Laboratory of High Performance Nontraditional Manufacturing, College of Mechatronics and Control Engineering, Shenzhen University, Shenzhen, 518060, China

[b] Department of Electrical Engineering, Yuan Ze University, Taoyuan, Taiwan, China

ARTICLE INFO

Keywords:
Bulk amorphous alloys
Ductility and strength
Relaxation enthalpy
Nanocrystallization
Intermittent high-frequency vibration loading

ABSTRACT

Intermittent high-frequency vibration loading is introduced into the $Zr_{41.2}Ti_{13.8}Cu_{12.5}Ni_{10}Be_{22.5}$ bulk amorphous alloy as an ultrashort time, easy-to-obtain, nondestructive physical method to adjust its atomic arrangement and shear deformation behavior. It is found that the method of intermittent high-frequency vibration loading can make the ductility and strength of the bulk amorphous alloys increase quickly within 4 s, increasing to 5.3% and 2240 MPa, respectively. And there is a mechanical power threshold of approximately 0.43 kJ/mol. Apart from the as-cast sample, when it is less than this threshold, with the increase of amplitude and pre-pressure, the relaxation enthalpy of IHF-treated samples increases, the ductility increases, but the compressive yield strength is basically unchanged, and there is basically no precipitation of nanocrystals at the same time. When it is greater than the threshold, as the amplitude and pre-pressure increase, the relaxation enthalpy decreases, nanocrystals precipitate, the ductility and the compressive yield strength begin to decrease. Both the increase in free volume content and the appearance of nanocrystals will lead to an increase in the critical stress of the first ejection event, thereby simultaneously increasing the ductility and yield strength. It is also found that the increase in free volume content is the main factor for the increase in ductility and strength, and the appearance of nanocrystals is a secondary factor. Our findings provide a new ultrashort time method for overcoming the strength-ductility trade-off dilemma.

1. Introduction

Bulk amorphous alloys have many excellent properties, such as high strength, high hardness, and high wear resistance, but their room temperature ductility is extremely poor, which affects their wide use [1]. At present, many scholars have studied methods to improve the room temperature ductility of amorphous alloys. One method is to increase the elastic modulus and Poisson's ratio by designing the element ratio of the amorphous alloy so that the shear band will continue to expand instead of cracking. Both W.L. Johnson et al. [2] and Y.H. Liu et al. [3] used this method to increase the strain of Pt-based or Zr-based bulk amorphous alloys, and the strain amount reached 20% and 150%, respectively. The second method is to change the internal atomic arrangement by elastic loading [4], high-temperature creep [5] or thermal cycling [6] to increase both the amount of free volume and the room temperature ductility. The third method is to introduce multiple small shear bands through local plastic deformation, e.g., cold rolling [7], severe plastic deformation [8], high-pressure torsion [9] and ball milling [10]. When the amorphous alloy is subjected to an external force again, the expansion of a large number of shear bands induces the generation of new shear bands, thereby improving the room temperature ductility.

Free volume theory has confirmed that the action of shear stress can induce a large amount of free volume inside bulk amorphous alloys. For example, Ogta S et al. [11] simulated the cluster structure of $Cu_{57}Zr_{43}$ bulk amorphous alloys under elastic loading by molecular dynamics, and the free volume content increased. However, the current elastic loading method takes several hours or days, and the time is too long. During this period, a relaxation effect will inevitably occur, thereby reducing the free volume content.

In addition, an increasing number of studies have shown that the performance of bulk amorphous alloys can be controlled by adjusting the energy state. For example, Z.Y. Liu et al. [12] previously found that the free volume content of Zr-based bulk amorphous alloys can be

* Corresponding author.
E-mail address: louyan@szu.edu.cn (Y. Lou).

https://doi.org/10.1016/j.intermet.2022.107467
Received 4 September 2021; Received in revised form 26 November 2021; Accepted 10 January 2022
Available online 16 January 2022

quickly increased by the ultrasonic vibration precompression method, thereby improving their plasticity. Ultrasonic energy reduces the activation energy of atomic transitions and drives the atoms to high energy with elastic vibration energization, thereby introducing more free volume and rheological units to induce shear bands. At the same time, ultrasonic vibration largely avoids time-dependent structural relaxation and crystallization, thereby avoiding the risk of crystallization during the traditional heat treatment process. However, T. Ichitsubo et al. [13] have discovered that crystallization occurs when the bulk amorphous alloy is vibrated ultrasonically. G. Kumar et al. [14] found that amorphous brittleness is caused by crystallization, and W. Zhai et al. [15] found that ultrasound-induced nanocrystals can simultaneously increase the compressive plasticity and yield strength of bulk amorphous alloys. Therefore, the effect of ultrasonic vibration on the microstructure and properties of bulk amorphous alloys is very complicated. There is currently an urgent problem is to study how ultrasonics can overcome the dilemma of the strength-ductility trade-off of bulk amorphous alloys.

The effects of the coupling of the ultrasonic amplitude and pre-pressure on the microstructure and properties of Zr-based bulk amorphous alloys during the intermittent high-frequency (IHF) vibration loading process were quantitatively analyzed. It was found that the method of IHF vibration loading can make the ductility and strength of the bulk amorphous alloys increase quickly within 4 s. At the same time, IHF vibration loading dual external field has a mechanical power threshold. When the value of the mechanical power is less than this threshold, as the amplitude and pre-pressure increase, this power increases, the relaxation enthalpy of IHF-treated samples increases, and the ductility increases, but the compressive yield strength is basically unchanged, and there is basically no precipitation of nanocrystals. When the power is greater than this threshold, as the amplitude and pre-pressure increase, the mechanical power increases, resulting in excessive energy imparted to the amorphous alloy, reducing the amorphous relaxation enthalpy. The precipitation of nanocrystals occurs, and the ductility and compression yield strength begin to decrease, but which are greater than those of the as-cast sample. Based on the experimental results, the softening mechanism and strengthening mechanism of IHF vibration loading is thoroughly discussed.

2. Experimental materials and methods

2.1. Preparation of test materials

An ingot of $Zr_{41.2}Ti_{13.8}Cu_{12.5}Ni_{10}Be_{22.5}$ (composition is given in atomic percentage) was selected for the experiment. All elements were made of pure metals with a concentration higher than 99% and were melted in a vacuum arc melting furnace under the protection of argon to prepare a master alloy. The master alloy was repeatedly melted approximately 5 times to ensure the uniform distribution of the elements. The columnar bulk amorphous alloy with a diameter of ∅ 2 × 70 mm was prepared by suction casting with a water-cooled copper mold and then was cut into a round rod with a length of 3.0 mm. After the sample was annealed at 560 K for 12 h, the relaxation enthalpy decreased by 52%, implying that the amorphous alloy sample obtained a uniform initial state at this time [16]. Finally, both ends were smoothed with fine sandpaper.

2.2. Design of the intermittent high-frequency vibration loading experiment scheme

The IHF vibration loading experiment platform was formed by a universal material experiment machine (Zwick Z050, Zwick Roell Group, Ulm, Germany) equipped with an ultrasonic module. The ultrasonic module used in this experiment was composed of a support frame, an ultrasonic generator, an ultrasonic timer, a transducer, a horn and an ultrasonic punch. The ultrasonic generator converts electrical energy into mechanical vibration, amplifies it to the required amplitude through the horn, and finally transmits the ultrasonic vibration to the sample of bulk amorphous alloys through the periodic impact of the punch.

The support frame was fixed on the moving beam of the universal testing machine, and the moving speed was controlled by a computer. At the same time, the force and displacement sensors recorded the experimental data in real time. An ultrasonic timer was used to achieve the ratio of ultrasonic work to intermittent time. When the punch pressed down to contact the sample, the pre-pressure increased to the set value, and the ultrasonic timer was turned on for intermittent ultrasonic action on amorphous samples.

2.3. Test and analysis methods

The strain rate of the IHF vibration loading experiment was 3×10^{-4} s^{-1}, the ultrasonic frequency was 20 kHz, and the ultrasonic intermittent ratio was 1:1; that is, the ultrasonic loading was 1 s, the interval was 1 s, the ultrasonic loading time was 4 s in the whole compression process, the ultrasonic amplitudes were 18 μm, 26 μm and 35 μm, and the pre-pressure values were 96 MPa, 207 MPa and 319 MPa, respectively. For each set of process parameters, IHF loading treatment was repeated for 5 samples to ensure the repeatability of the evaluation results.

X-ray diffraction (XRD) was used to detect whether the samples are amorphous. The equipment model of the diffractometer was Bruker D8-AA25 (Bruker, Karlsruhe, Germany). The X-ray incidence range was set to 20°–80°, the step length was 0.02°, and the Cu-Ka ray wavelength λ = 1.5418 Å.

A differential scanning calorimeter (DSC) instrument (DSC-8000, PerkinElmer, Poulsbo, WA, USA) was used to detect the relaxation enthalpy of the samples. In all cases, the samples were first heated to a fully crystalline state and then cooled to room temperature with a heating rate of 0.33 K/s, a cooling rate of 1.66 K/s, and heating to 600 °C.

Scanning electron microscopy (SEM) was performed using a Philips XL30 instrument (Philips Company, Amsterdam, Netherland). The focus was on the evolution of the shear band of the fracture surface.

A Hysitron TI-950 nanoindenter (Hysitron Inc., Minneapolis, USA) was used to conduct nanoindentation experiments on the sample surface. The indentation speed was 0.2 nm s^{-1}, and the peak load was 8 mN. To ensure that the indentations did not affect each other, the interval between adjacent indentations was 5 μm and measured in a 5 × 5 dot matrix for each sample. To ensure the accuracy of the experiment, before the experiment, the bulk amorphous alloy samples were polished to ensure smoothness, and at the same time, they were subjected to stress annealing for 30 min in a vacuum environment.

Transmission electron microscopy (TEM, JEM-2100F, JEOL Ltd., Tokyo, Japan), with an accelerating voltage of 200 kV, was used to observe the microstructure of the sample. The thin slices were cut from the sample, mechanically ground to a thickness of 0.5 mm and mounted on a TEM copper grid.

3. Results

The XRD pattern in Fig. 1 shows that, except for the sample with IHF vibration loading at an amplitude greater than 26 μm or a pre-pressure greater than 207 MPa, the as-cast and other IHF-treated samples have broad diffraction peaks, indicating that these materials have a typical amorphous structure. Notably, the IHF-26-207 sample begins to exhibit a weak peak. When the pre-pressure was increased to 319 MPa, sample IHF-26-319 showed multiple faint peaks. A comparison with the standard XRD template shows that $CuZr_2$ and $Be_{13}Zr$ nanocrystals were precipitated.

DSC experiments were carried out, and the thermodynamic parameters of the as-cast and three typical IHF-treated samples were recorded in detail, as shown in Fig. 2. The corresponding glass transition temperature T_g, crystallization temperature T_x and crystallization peak

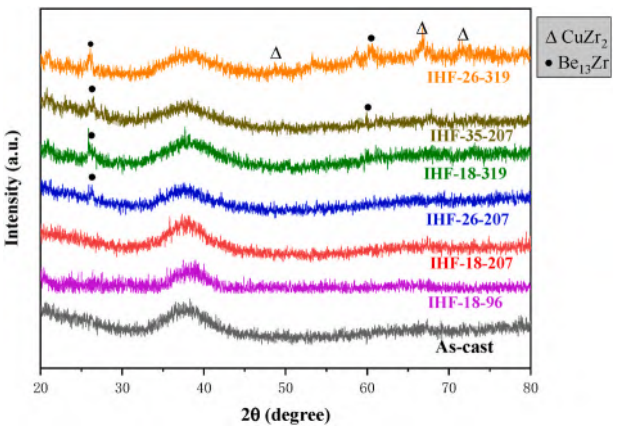

Fig. 1. XRD patterns of the as-cast and IHF-treated $Zr_{41.2}Ti_{3.8}Cu_{12.5}Ni_{10}Be_{22.5}$ alloy samples.

temperature T_p of the four samples are similar. However, it is worth noting that the relaxation enthalpies of the four samples change significantly. When the pre-pressure is 207 MPa, with increasing ultrasonic amplitude, the relaxation enthalpy △H clearly increases from 2.087 J/g to 11.701 J/g. Since the change of △H reflects the disorder of atomic arrangement [17], it can be used to qualitatively study the change of free volume content in amorphous alloys. △H is directly proportional to the free volume content [18]. After the ultrasonic vibration is excited, △H increases by approximately 5.6 times, indicating that the disorder of the atomic arrangement increases during the IHF vibration treatment, and the free volume content increases. It can also be noticed from Fig. 2 that when the amplitude increases from 18 μm to 26 μm, △H increases by 8.014 J/g, indicating that the larger the amplitude is, the greater the free volume content. However, when the amplitude is 26 μm, as the pre-pressure increases from 207 MPa to 319 MPa, the relaxation enthalpy drops significantly to 6.222 J/g, indicating that the free volume content is reduced at this time, the atoms are tightly arranged, and amorphous matrix crystallization may occur.

To understand the effect of IHF treatment on the microstructure of the $Zr_{41.2}Ti_{3.8}Cu_{12.5}Ni_{10}Be_{22.5}$ bulk amorphous alloy, a TEM study was carried out. From the TEM images shown in Fig. 3 (a)-(c), the as-cast samples and the IHF-18-207 and IHF-26-207 samples demonstrate uniform contrast with no obvious lattice fringes and a labyrinth pattern in all directions. The corresponding selected area electron diffraction (SAED) pattern shown in the illustration is composed of a wide diffraction halo, indicating a typical characteristic amorphous structure, which is basically consistent with the XRD experimental results of the same sample in Fig. 1.

Fig. 3 (d) is the TEM image of sample IHF-26-319. In addition to the labyrinth pattern, there are many dark "band-like" regions with a visible length of 20–50 nm that are uniformly precipitated from the amorphous matrix. As shown in the illustration, the diffusive SAED ring pattern is superimposed with some diffraction points, indicating that the sample matrix is still a typical characteristic amorphous structure, but nanocrystalline grains occasionally appear. Enlarging the red frame area marked in Fig. 3 (d), shows that this part is a typical maze pattern (Fig. 3 (e)). The enlarged marked yellow frame area shows that the mixture of order clusters and nanocrystals is distributed on an amorphous matrix (Fig. 3 (f)).

The SAED pattern corresponding to the blue frame marked in Fig. 3 (f) shows typical diffraction points, indicating that this part is a single crystal structure (Fig. 3 (g)). An enlarged pattern is performed in Fig. 3 (g), and a pattern composed of sharp diffraction spots and diffuse halos along the [0 1 $\bar{3}$] crystal axis plane is obtained (Fig. 3 (h)). According to the XRD results of sample IHF-26-319 in Fig. 1, this sample may precipitate $CuZr_2$ and $Be_{13}Zr$ crystal phases. Therefore, through the calculation method from the literature [15], the distance and the included angle between the red circle and three nearby yellow circles are calculated. The results are compared with the standard $CuZr_2$ and $Be_{13}Zr$ TEM results, and the nanocrystal is determined to be the $CuZr_2$ phase. The cubic lattice parameters are a = b = 0.311 nm, c = 0.089 nm, and α = β = γ = 90°. The crystal plane indices represented by the three yellow circles are (0 3 $\bar{1}$), ($\bar{2}$ 0 0) and ($\bar{2}$ 3 $\bar{1}$).

Previous studies also reported the formation of such $CuZr_2$ nanocrystals. I. Kaban et al. [19] simulated the topological and chemical short-range order of $Zr_{47.5}Cu_{47.5}Al_5$ amorphous alloys and found that the $Cu_{10}Zr_7$, $CuZr_2$ and CuZr phases precipitated in sequence. The atomic ratio of Zr in the $Zr_{41.2}Ti_{13.8}Cu_{12.5}Ni_{10}Be_{22.5}$ bulk amorphous alloy is more than twice that of Cu. Therefore, it can be understood that the $CuZr_2$ phase preferentially precipitates in bulk amorphous alloys excited by IHF vibration loading.

To study the effect of the IHF on the mechanical properties of the samples, uniaxial compression tests were carried out at room temperature. Fig. 4 (a) shows the typical compressive stress-strain curves of the as-cast and IHF-treated samples.

The black line represents the compressive stress-strain curve of the as-cast sample, which shows a brittle structure (Fig. 4 (a)). The ultimate compressive stress determined by the first platform in the curve is 1793 MPa. After IHF treatment, it was found that the ultimate compressive

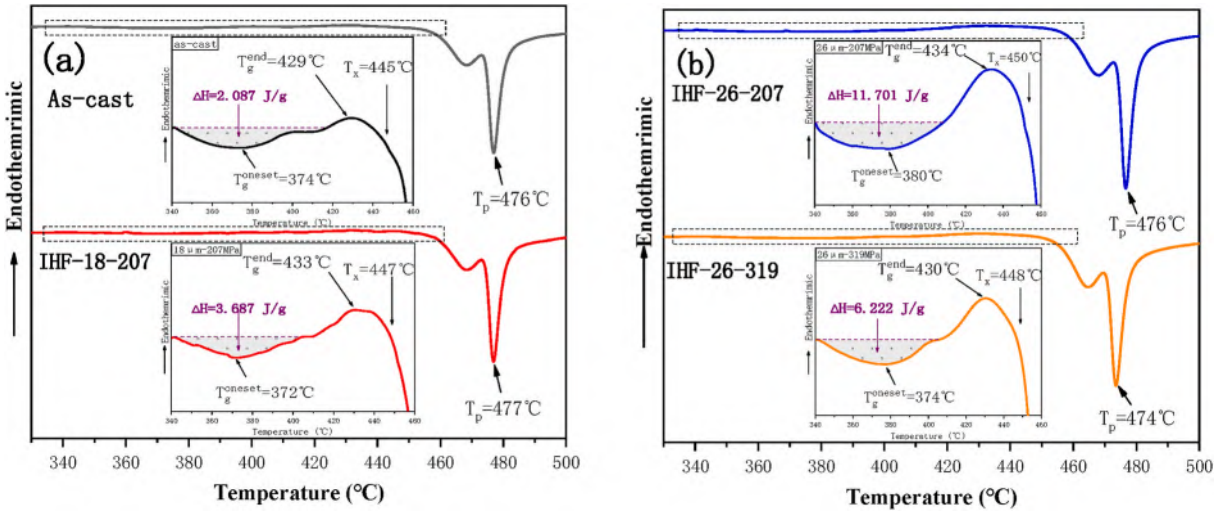

Fig. 2. DSC traces on heating in temperature range from 330 to 500 °C: (a) As-cast and IHF-18-207 samples; (b) IHF-26-207 and IHF-26-319 samples.

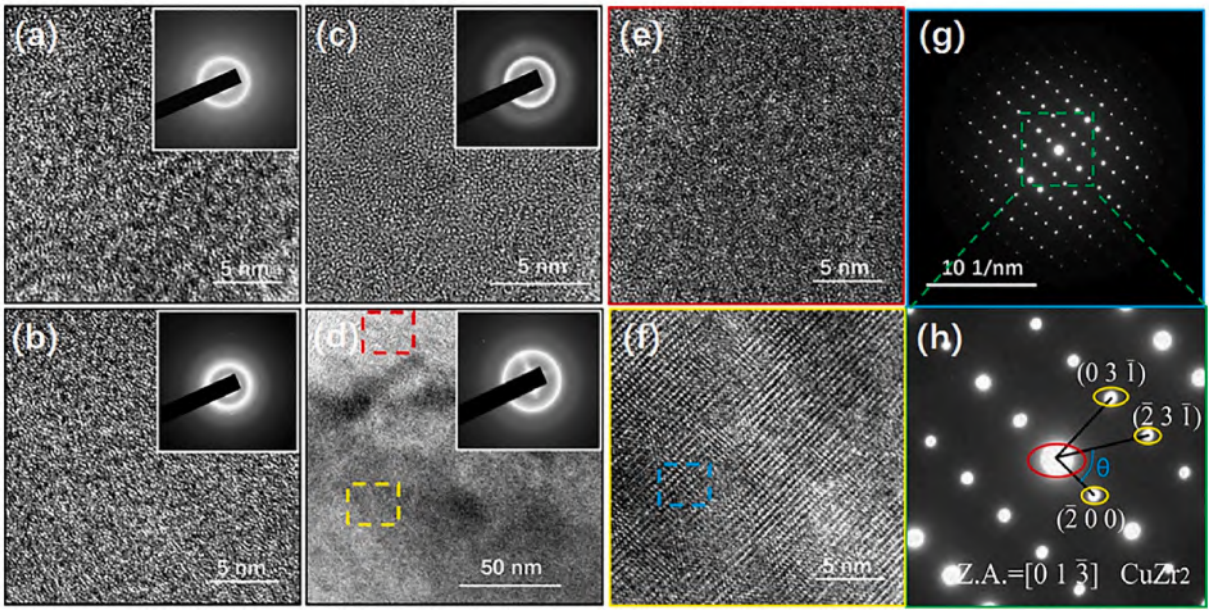

Fig. 3. Microstructures of $Zr_{41.2}Ti_{13.8}Cu_{12.5}Ni_{10}Be_{22.5}$ bulk amorphous alloy: TEM and the corresponding SAED patterns for (a) the as-cast samples; (b) IHF-18-207 samples; (c) IHF-26-207 samples; (d) IHF-26-319 samples; (e) TEM image showing a typical maze pattern of red frame area in (d); (f) TEM image showing nanocrystals embedded in amorphous matrix of yellow frame area in (d); (g) the corresponding SAED pattern to the blue frame area in (f); (h) the enlarged pattern to the green frame area in (g).

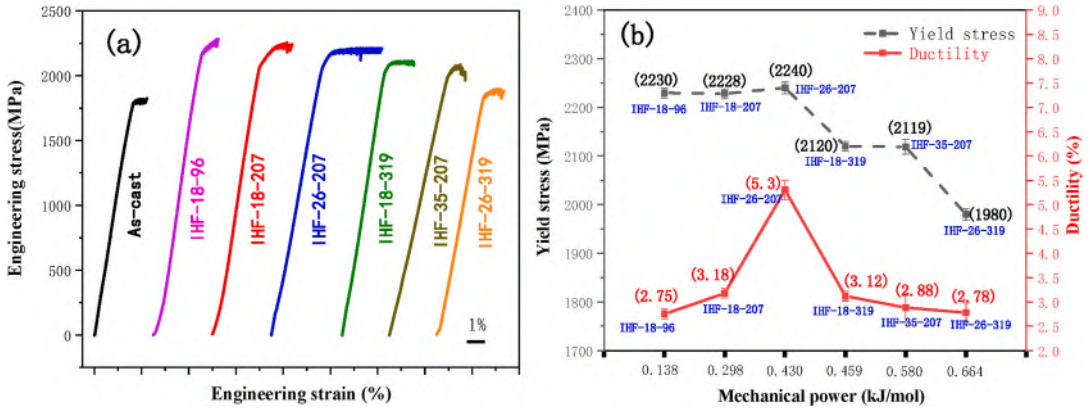

Fig. 4. Effects of IHF vibration loading excitation on the macroscopic mechanical behavior of $Zr_{41.2}Ti_{13.8}Cu_{12.5}Ni_{10}Be_{22.5}$ bulk amorphous alloy: (a) strain-stress curves in quasi-static compression test; (b) the relationship between the mechanical power and the ductility and yield strength of the IHF-treated samples.

stress and ductility of all IHF samples increased. The blue line represents that the yield stress of the IHF-26-207 sample increased to 2240 MPa when the amplitude was 26 μm and the pre-pressure was 207 MPa, the ultimate compressive stress also increased to 2255 MPa, and the maximum ductility was 5.3%. The orange line represents the yield stress and ultimate compressive stress of the IHF-26-319 sample when the amplitude is 26 μm and the pre-pressure is 319 MPa. Compared with the IHF-26-207 sample, the yield stress and ultimate compressive stress values are reduced to 1980 MPa and 1997 MPa, respectively. The increase in pre-pressure reduces the strength of the sample, and the maximum ductility is also reduced to 2.78%. These results show that although the IHF-treated $Zr_{41.2}Ti1_{3.8}Cu_{12.5}Ni_{10}Be_{22.5}$ bulk amorphous alloy can excite the best ductility and strength, there is a threshold.

The punch mechanical power is used to calculate this threshold. The mechanical power of the IHF vibration loading is as Eq. (1).

$$W = F_s \times (f \cdot t \cdot A) \tag{1}$$

where F_s is the pre-pressure, MPa; f is the frequency, ($f = 20\ kHz$); t is the ultrasonic action time, which takes 4 s; and A is the amplitude, μm.

Fig. 4 (b) shows the relationship between the mechanical power and the ductility and yield strength of the IHF-treated samples. The ductility is the largest when the power is approximately 0.43 kJ/mol. If the power is too large or too small, then the ductility will be reduced. However, the change rule of the compression yield strength is different. Apart from the as-cast sample, it is found when the power is less than 0.43 kJ/mol, the yield strength of IHF-treated samples basically changes little. When it is greater than 0.43 kJ/mol, the yield strength will decrease slightly. Therefore, the best ductility and strength threshold for the IHF treatment of the $Zr_{41.2}Ti_{13.8}Cu_{12.5}Ni_{10}Be_{22.5}$ bulk amorphous alloy is approximately 0.43 kJ/mol.

Fig. 5 shows the typical side surface morphology of the as-cast, IHF-26-207 and IHF-26-319 samples. Initially, only two straight and well-separated shear bands can be observed near the fracture surface of the as-cast sample (Fig. 5 (a)). In contrast, a significant number of shear bands, including secondary shear bands, are formed around the samples subjected to IHF vibration loading. However, compared with the IHF-26-207 sample, the number of shear bands is clearly reduced in the

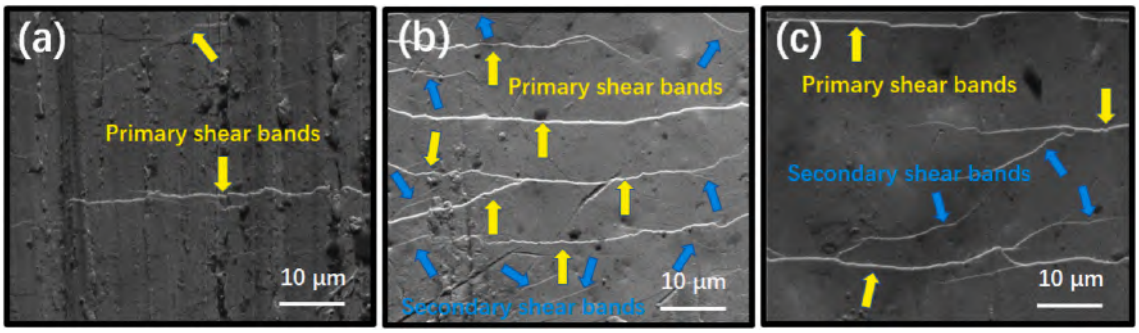

Fig. 5. SEM views of the fracture surface appearance for (a) the as-cast sample with primary shear bands; (b) IHF-26-207 sample with multiple shear bands; and (c) IHF-26-319 sample with multiple shear bands.

IHF-26-319 sample (Fig. 5 (c)). The formation of such high-density and widely distributed shear bands excited by the IHF treatment is the reason for the ductility change in the $Zr_{41.2}Ti_{13.8}Cu_{12.5}Ni_{10}Be_{22.5}$ bulk amorphous alloy. The shear band results are consistent with the change in ductility in the volumetric compression test.

The micromechanical properties related to the structural characteristics of the $Zr_{41.2}Ti_{13.8}Cu_{12.5}Ni_{10}Be_{22.5}$ bulk amorphous alloy were also studied by nanoindentation tests. Fig. 6 shows three typical depth-load curves of the as-cast, IHF-26-207 and IHF-26-319 samples. Clearly, the critical load (indicated by the arrow) of the first sudden ejection event refers to the initial yield due to the formation of the shear band, which becomes higher after IHF treatment. Fig. 6 (b) shows the average critical load at the first yield point on the depth-load curve. The average critical loads after IHF treatment increase toward a higher value as a whole, which is in good agreement with the typical results in Fig. 6 (a). The findings show that after IHF treatment, the $Zr_{41.2}Ti_{13.8}Cu_{12.5}Ni_{10}Be_{22.5}$ bulk amorphous alloy requires a higher critical stress to trigger the first shear band event. In the above three samples, the IHF-26-207 sample requires the highest critical stress to trigger the first shear band event. The nanoindentation results are consistent with the change in yield strength in the volume compression test.

4. Discussion

From the above structural characteristics and the results of macro- and micromechanical properties, it is concluded that IHF treatment can overcome the ductility-strength trade-off of bulk amorphous alloys. The free volume content, and the volume fraction, size and distribution of crystallites are crucial to the mechanical properties of the crystal-amorphous composition [12,20].

The increase in the free volume content may improve the ductility of bulk amorphous alloys in the following four aspects. First, the IHF mechanical power can reduce the activation energy of atomic transitions, and with vibration energization, the atoms are driven to high energy, thereby introducing more free volume and flow units to induce shear bands [12]. Second, a higher free volume content means that there are more disordered regions in the short-range arrangement of atoms, which increases the instability of the local topology. Under the action of external forces, atoms have more room to move freely, and it is also conducive to the connected seepage of adjacent flow units [21]. There is low deformation resistance, prompting stable rheological changes of atoms. Third, if the free volume content is large, the viscosity of bulk amorphous alloys is low, and the atoms can easily diffuse, thereby increasing the fluidity and ductility. Finally, as the free volume content increases, it is easy to form a secondary shear zone locally through local softening [22], which can block the expansion of the main shear zone.

On the other hand, the influence of nanocrystals on the ductility of bulk amorphous alloys is mainly due to the high-strength $CuZr_2$ nanocrystals, which can hinder the growth of shear bands and cracks. First, the nanocrystals distributed along the shear bands play a role in the stress concentration, and the new shear bands tend to nucleate, grow and diffuse at the interface between the matrix and the nanocrystals [15]. The newly formed secondary shear zone and the wing-shaped shear zone form a net, which can be expanded and mixed with other shear zones to maintain the increasing strain during the compression deformation process. Second, the growth of nanocrystals leads to an increase in viscosity [23]. The direction of shear deformation is changed to micro-zones with a relatively low crystallization fraction to render the deformation more homogenous [24]. As a result, the branching of the regenerative shear zone delays the expansion of the main shear zone, prompting the atoms to undergo sufficient and stable rheological changes. However, the presence of nanocrystals leads to an increase in the tightly arranged regions of local atoms, and the free volume content will inevitably decrease. Although nanocrystals can delay the expansion

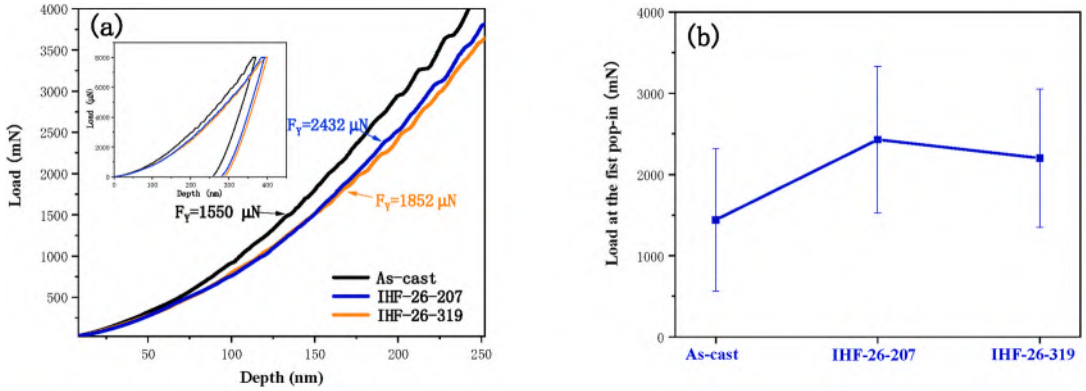

Fig. 6. Nanoindentation tests on $Zr_{41.2}Ti_{13.8}Cu_{12.5}Ni_{10}Be_{22.5}$ bulk amorphous alloy: (a) typical nanoindentation load-depth curves of the samples in as-cast state and IHF-26-207 and IHF-26-319; (b) average critical load at the first pop-in event.

of the secondary shear band, the overall viscosity of bulk amorphous alloys increases. Compared with the samples without nanocrystals, its ductility decreases.

Therefore, the above mentioned combination of the free volume content and nanocrystals avoids catastrophic fracture of bulk amorphous alloys at room temperature. From the perspective of the threshold of mechanical power furtherly, when it is less than the power threshold, almost no nanocrystals are precipitated on the amorphous matrix. At this time, as the power increases, the free volume content increases and the ductility increases; and after the threshold is exceeded, it is found that as the power increases, nanocrystals appear and gradually increase, the free volume content decreases, and the ductility decreases. Thence, the increase in free volume content plays a major role in improving the ductility of bulk amorphous alloys, and the formation of $CuZr_2$ nanocrystals may play a secondary role in ductility.

In addition, it can be seen from Fig. 2 (b) and Figs.5 (b)–(c) that the increase in the free volume content on the amorphous matrix result in a significant increase in the secondary shear bands. And the orientation of the shear band is more disordered. The hard-oriented secondary shear bands will restrict the expansion of the soft-oriented shear bands and increase the deformation resistance. Secondly, the dispersion of $CuZr_2$ on the amorphous matrix act as a reinforcing phase like "pinning", slowing down the propagation of the shear band. Therefore, in above both cases, a higher stress is required to activate the new shear zone. Both the free volume and nanocrystals help to increase the yield stress and ultimate compressive stress. However, the sizes of the nanocrystals range from 20 to 50 nm. The molecular chains in this part of the region are arranged in an orderly manner, which causes the movement of the segment units to be hindered. Therefore, this region is prone to more cracks. Compared with the samples without nanocrystal precipitation, the samples with nanocrystal have a slightly lower strength.

5. Conclusion

In summary, we found that IHF vibration loading can promote the movement of atoms and lead to an increase in the free volume content and the formation of $CuZr_2$ nanocrystals dispersed on the $Zr_{41.2}Ti_{13.8}Cu_{12.5}Ni_{10}Be_{22.5}$ alloy glass matrix, thereby improving quickly the ductility and yield strength. And there is a mechanical power threshold of approximately 0.43 kJ/mol. When the value of the mechanical power is less than the threshold, as the power increases, the ductility of IHF-treated samples increases, and the yield strength does not change. When the power is greater than this threshold, both the ductility and the yield strength decrease. By overcoming the dilemma of the strength-ductility trade-off, we provide an ultrashort time, easy-to-obtain, nondestructive and low-cost technical method to strengthen and improve the ductility and strength of bulk amorphous alloys.

Author statement

This work investigates the unique features of bulk amorphous alloys treated by intermittent high-frequency (IHF) vibration loading at room temperature. We found that the method of intermittent high-frequency vibration loading can make the ductility and strength of the bulk amorphous alloys increase quickly within 4 s. It also explains the differences in the effects of different amplitudes and pre-pressures on the relaxation enthalpies and nanocrystals precipitation of bulk amorphous alloys, and how these differences can alter their ductility and strength. And our finding is an ultrashort time, easy-to-obtain, nondestructive and low-cost technical method for overcoming the strength-ductility trade-off dilemma.

Declaration of competing interest

The authors declare that they have no known competing financial interests or personal relationships that could have appeared to influence the work reported in this paper.

Acknowledgements

This work was supported financially by the Science and Technology Innovation Commission of Shenzhen (No. JCYJ20190808152409578), and the National Natural Science Foundation of China (Grant No. 52075342 and No. 51971149). In addition, the authors want to acknowledge the assistance on HRTEM observation received from the Electron Microscope Center of the Shenzhen University.

References

[1] Z. Huang, J. Fu, X. Li, W. Wen, H. Lin, Y. Lou, F. Luo, Z. Zhang, X. Liang, J. Ma, Ultrasonic-assisted rapid cold welding of bulk metallic glasses, Sci. China Mater. 7 (2021) 1–7.
[2] J. Schroers, W.L. Johnson, Ductile bulk metallic glass, Phys. Rev. Lett. 93 (25) (2004) 255506.
[3] Y.H. Liu, G. Wang, R.J. Wang, D.Q. Zhao, M.X. Pan, W.H. Wang, Super plastic bulk metallic glass at room temperature, Science 315 (5817) (2007) 1385–1388.
[4] M. Zhang, Y.M. Wang, F.X. Li, S.Q. Jiang, M.Z. Li, L. Liu, Mechanical relaxation-to-rejuvenation transition in a Zr-based bulk metallic glass, Sci. Rep. 7 (1) (2017) 625.
[5] R. Raghavan, K. Boopathy, R. Ghisleni, M.A. Pouchon, U. Ramamurty, J. Michler, Ion irradiation enhances the mechanical performance of metallic glasses, Scripta Mater. 62 (7) (2010) 462–465.
[6] W. Guo, Y. Shao, J. Saida, M. Zhao, S. Lu, S. Wu, Rejuvenation and plasticization of Zr-based bulk metallic glass with various Ta content upon deep cryogenic cycling, J. Alloys Compd. 795 (2019) 314–318.
[7] M.H. Lee, K.S. Lee, J. Das, J. Thomas, U. Kuhn, J. Eckert, Improved plasticity of bulk metallic glasses upon cold rolling, Scripta Mater. 62 (9) (2010) 678–681.
[8] W. Dmowski, Y. Yokoyama, A. Chuang, Y. Ren, M. Umemoto, K. Tsuchiya, A. Inoue, T. Egami, Structural rejuvenation in a bulk metallic glass induced by severe plastic deformation, Acta Mater. 58 (2) (2010) 429–438.
[9] F. Meng, K. Tsuchiya, M.J. Kramer, R.T. Ott, Reduction of shear localization through structural rejuvenation in Zr–Cu–Al bulk metallic glass, Mater. Sci. Eng. 765 (2019) 138304.
[10] Y. Sun, A. Concustell, A.L. Greer, Thermomechanical processing of metallic glasses: extending the range of the glassy state, Nat. Rev. Mater. 39 (2016) 16039.
[11] S. Ogata, F. Shimizu, J. Li, M. Wakeda, Y. Shibutani, Atomistic simulation of shear localization in Cu-Zr bulk metallic glass, Intermetallics 14 (8–9) (2006) 1033–1037.
[12] Y. Lou, X. Liu, X.L. Yang, Y. Ge, D.D. Zhao, H. Wang, L.C. Zhang, Z.Y. Liu, Fast rejuvenation in bulk metallic glass induced by ultrasonic vibration precompression, Intermatallics 118 (2020) 106687.
[13] T. Ichitsubo, E. Matsubara, T. Yamamot, H.S. Chen, N. Nishiyama, J. Saida, K. Anazawa, Microstructure of fragile metallic glasses inferred from ultrasound-accelerated crystallization in Pd-based metallic glasses, Phys. Rev. Lett. 95 (2005) 245501.
[14] G. Kumar, D. Rector, R.D. Conner, J. Schroers, Embrittlement of Zr-based bulk metallic glasses, Acta Mater. 57 (12) (2009) 3572–3583.
[15] W. Zhai, L.H. Nie, X.D. Hui, Y. Xiao, T. Wang, B. Wei, Ultrasonic excitation induced nanocrystallization and toughening of $Zr_{46.75}Cu_{46.75}Al_{6.5}$ bulk metallic glass, J. Mater. Sci. Technol. 45 (2020) 157–161.
[16] Z.G. Zhu, P. Wen, D.P. Wang, R.J. Xue, D.Q. Zhao, W.H. Wang, Characterization of flow units in metallic glass through structural relaxations, J. Appl. Phys. 114 (2013), 083512.
[17] S.E. Dang, G. Zhang, Z.Y. Li, Z.J. Yan, Y.T. Li, W. Liang, Variation of microstructure of $Zr_{60}Al_{15}Ni_{25}$ bulk amorphous alloy during rolling at room temperature, J. Alloys Compd. 479 (1–2) (2009) 15–17.
[18] A. Slipenyuk, J. Eckert, Correlation between enthalpy change and free volume reduction during structural relaxation of $Zr_{55}Cu_{30}Al_{10}Ni_5$ metallic glass, Scripta Mater. 50 (1) (2004) 39–44.
[19] I. Kaban, P. Jo'va'ri, B. Escher, D.H. Tran, G. Svensson, M.A. Webb, T.Z. Regier, V. Kokotin, B. Beuneu, T. Gemming, J. Eckert, Atomic structure and formation of CuZrAl bulk metallic glasses and composites, Acta Mater. 100 (2015) 369–376.
[20] Y. Wu, H. Wang, X.J. Liu, X.H. Chen, X.D. Hui, Y. Zhang, Z.P. Lu, Designing bulk metallic glass composites with enhanced formability and plasticity, J. Mater. Sci. Technol. 30 (2014) 566–575.
[21] M. Zhang, L. Liu, Y.M. Wu, Facilitation and correlation of flow in metallic supercooled liquid, J. Chem. Phys. 139 (16) (2013) 164508.
[22] L. Li, E.R. Homer, C.A. Schuh, Shear transformation zone dynamics model for metallic glasses incorporating free volume as state variable, Acta Mater. 61 (9) (2013) 3347–3359.
[23] I.M. Krieger, T.J. Dougherty, A mechanism for non-Newtonian flow in suspensions of rigid spheres, Trans. Soc. Rheol. 111 (1959) 137–152.
[24] K. Hajlaoui, A.R. Yavari, A. Lemoulec, W.J. Botta, F.G. Vaughan, J. Das, A.L. Greer, A. Kvick, Plasticity induced by nanoparticle dispersions in bulk metallic glasses, J. Non-Cryst. Solids 353 (2007) 327–331.